THE ASTROPHYSICAL JOURNAL, 464:L21–L24, 1996 June 10

ANGULAR POWER SPECTRUM OF THE COSMIC MICROWAVE BACKGROUND ANISOTROPY SEEN BY THE *COBE*[1] DMR

E. L. WRIGHT,[2] C. L. BENNETT,[3] K. GÓRSKI,[4,5] G. HINSHAW,[4] AND G. F. SMOOT[6]
Received 1996 January 11; accepted 1996 March 21

ABSTRACT

The angular power spectrum estimator developed by Peebles and Hauser & Peebles has been modified and applied to the 4 yr maps produced by the *COBE* DMR. The power spectrum of the observed sky has been compared to the power spectra of a large number of simulated random skies produced with noise equal to the observed noise and primordial density fluctuation power spectra of power-law form, with $P(k) \propto k^n$. The best-fitting value of the spectral index in the range of spatial scales corresponding to spherical harmonic indices $3 \leq \ell \lesssim 30$ is an apparent spectral index $n_{\rm app} = 1.13^{+0.3}_{-0.4}$ which is consistent with the Harrison-Zeldovich primordial spectral index $n_{\rm pri} = 1$. The best-fitting amplitude for $n_{\rm app} = 1$ is $\langle Q^2_{\rm rms}\rangle^{0.5} = 18\ \mu$K.

Subject headings: cosmic microwave background — cosmology: observations

1. INTRODUCTION

The spatial power spectrum of primordial density perturbations $P(k)$, where k is the spatial wavenumber, provides evidence about processes occurring very early in the history of the universe. In the first moments after the big bang, the horizon scale ct corresponds to a current scale that is much smaller than galaxies, so the assumption of a scale-free form for $P(k)$ on large scales is natural, which implies a power law $P(k) \propto k^n$. Harrison (1970), Zeldovich (1972), and Peebles & Yu (1970) all pointed out that the absence of tiny black holes implies $n \lesssim 1$, while the large-scale homogeneity implied by the near isotropy of the cosmic microwave background radiation (CMBR) requires $n \gtrsim 1$. Thus, the prediction of a Harrison-Zeldovich or $n = 1$ form for $P(k)$ by an analysis that excludes all other possibilities is an old one. This particular scale-free power law is scale-invariant because the perturbations in the metric (or gravitational potential) are independent of the scale. The inflationary scenario (Starobinsky 1980; Guth 1981) proposes a tremendous expansion of the universe (by a factor $\gtrsim 10^{30}$) during the inflationary epoch, which can convert quantum mechanical fluctuations on a microscopic scale during the inflationary epoch into gigaparsec-scale structure now, giving an almost scale-invariant spectrum with $n \approx 1$ (Bardeen, Steinhardt, & Turner 1983). Bond & Efstathiou (1987) show that the expected variance of the coefficients $a_{\ell m}$ in a spherical harmonic expansion of the CMBR temperature, given a power-law power spectrum $P(k) \propto k^n$, is $\langle a^2_{\ell m}\rangle \propto \Gamma[\ell + (n-1)/2]/\Gamma[\ell + (5-n)/2]$ for $\ell < 40$. Thus, a study of the angular power spectrum of the CMBR can be used to place limits on the spectral index n and test the inflationary prediction of a spectrum close to the Harrison-Zeldovich spectrum with $n = 1$.

The angular power spectrum contains the same information as the angular correlation function, but in a form that simplifies the visualization of fits for the spectral index n. Furthermore, the off-diagonal elements of the covariance matrix have a smaller effect for the power spectrum than for the correlation function. However, with partial sky coverage, the multipole estimates in the power spectrum are correlated, and this covariance must be considered when analyzing either the correlation function or the power spectrum.

The power spectrum of a function mapped over the entire sphere can be derived easily from its expansion into spherical harmonics, but for a function known only over part of the sphere this procedure fails. Wright et al. (1994a) have modified a power-spectral estimator from Peebles (1973) and Hauser & Peebles (1973) that allows for partial coverage, and they have applied this estimator to the DMR maps of CMBR anisotropy. We report here on the application of these statistics to the DMR maps based on all 4 yr of data (Bennett et al. 1996). Monte Carlo runs have been used to calculate the mean and covariance of the power spectrum. Fits to estimate $\langle Q^2_{\rm rms}\rangle^{0.5}$ and n by maximizing the Gaussian approximation to the likelihood of the angular power spectrum are discussed in this Letter. Since we only consider power-law power spectrum fits in this paper, we use Q as a shorthand for $\langle Q^2_{\rm rms}\rangle^{0.5}$ or $Q_{\rm rms-PS}$, which is the rms quadrupole averaged over the whole universe, based on a power-law fit to many multipoles. $\langle Q^2_{\rm rms}\rangle^{0.5}$ should not be confused with the actual quadrupole of the high Galactic latitude part of the sky observed from the Sun's location within the universe, which is the $Q_{\rm rms}$ discussed by Bennett et al. (1992).

2. ESTIMATING THE ANGULAR POWER SPECTRUM

Wright et al. (1994a) have discussed the modification of the Hauser-Peebles angular power-spectrum estimator for use on CMBR anisotropy maps. To allow for the cutting out of the

[1] The National Aeronautics and Space Administration/Goddard Space Flight Center (NASA/GSFC) is responsible for the design, development, and operation of the *Cosmic Background Explorer* (*COBE*). Scientific guidance is provided by the *COBE* Science Working Group. GSFC is also responsible for the development of the analysis software and for the production of the mission data sets.

[2] UCLA Astronomy, P.O. Box 951562, Los Angeles, CA 90095-1562; wright@astro.ucla.edu.

[3] Laboratory for Astronomy and Solar Physics, Code 685, NASA/GSFC, Greenbelt, MD 20771.

[4] Hughes STX Corporation, Laboratory for Astronomy and Solar Physics, Code 685, NASA/GSFC, Greenbelt, Maryland 20771.

[5] On leave from Warsaw University Observatory, Aleje Ujazdowskie 4, 00-478 Warsaw, Poland.

[6] Department of Physics, Lawrence Berkeley Laboratory, Space Sciences Laboratory, and Center for Particle Astrophysics, Building 50-351, University of California, Berkeley, CA 94720.

Galactic plane, new basis functions are defined using a modified inner product:

$$\langle fg \rangle = \frac{\sum_{j=1}^{N} w_j f_j g_j}{\sum_{j=1}^{N} w_j}, \quad (1)$$

where j is an index over pixels and w_j is the weight pixel^{-1}. In the Galactic plane cut, $w_j = 0$. We have *not* used weights proportional to the number of observations, so $w_j = 1$ outside of the Galactic plane cut. The custom Galactic cut used in this paper basically follows $\sin |b| = 1/3$, with extra cuts added in Sco-Oph and Orion (Bennett et al. 1996). A total of 3881 pixels are used, or 63% of the sky.

The modified Hauser-Peebles method in Wright et al. (1994a) used basis functions, defined using

$$G_{\ell m} = F_{\ell m} - \frac{F_{00}\langle F_{00} F_{\ell m}\rangle}{\langle F_{00} F_{00}\rangle} - \sum_{m'=-1}^{1} \frac{F_{1m'}\langle F_{1m'} F_{\ell m}\rangle}{\langle F_{1m'} F_{1m'}\rangle}, \quad (2)$$

where the $F_{\ell m}$ are real spherical harmonics and the inner product $\langle fg \rangle$ is defined over the cut sphere. These functions $G_{\ell m}$ are orthogonal to monopole and dipole terms on the cut sphere. We call this the MD method since the basis functions are orthogonal to the monopole and dipole. Let the MDQ method use basis functions orthogonal to the monopole, dipole, and quadrupole:

$$G'_{\ell m} = F_{\ell m} - \frac{F_{00}\langle F_{00} F_{\ell m}\rangle}{\langle F_{00} F_{00}\rangle} - \sum_{m'=-1}^{1} \frac{F_{1m'}\langle F_{1m'} F_{\ell m}\rangle}{\langle F_{1m'} F_{1m'}\rangle} - \sum_{m'=-2}^{2} \frac{F_{2m'}\langle F_{2m'} F_{\ell m}\rangle}{\langle F_{2m'} F_{2m'}\rangle}. \quad (3)$$

In this paper we have used the MDQ method, so our results for $\ell \geq 3$ are completely independent of the quadrupole in the map. We have also tabulated the power in $\ell = 2$, which is computed with G'_{2m}'s which are orthogonal to the monopole, dipole, and those components of the quadrupole which occur earlier in the sequence than m. Because the Galactic cut used is not a straight $|b|$ cut, the different F_{2m}'s are not quite orthogonal, and the definition of G'_{2m} depends slightly on the ordering of the $F_{\ell m}$'s. We use the ordering 1, $\cos\phi$, $\cos 2\phi$, $\sin\phi$, $\sin 2\phi$. With these basis functions we compute the power spectrum estimators

$$\frac{T_\ell^2}{2\ell + 1} = \frac{\sum_{m=-\ell}^{\ell} \langle G'_{\ell m} T\rangle^2}{\sum_{m=-\ell}^{\ell} \langle G'_{\ell m} G'_{\ell m}\rangle}, \quad (4)$$

which are quadratic functions of the maps. Note that for full sky coverage, the expected value $\langle T_\ell^2 \rangle$ is the variance of the sky in order ℓ or $(2\ell + 1)C_\ell/4\pi$, but for partial sky coverage the response of T_ℓ^2 to inputs with $\ell' \neq \ell$ causes $\langle T_\ell^2 \rangle$ to be larger than the order ℓ sky variance. Table 1 of Wright et al. (1994a) shows the input-output matrix for a straight 20° cut, while Table 1 shows the ℓ', $\ell \leq 9$ portion of the input-output matrix for the custom Galaxy cut.[7] The jump in Figure 1 at $\ell = 5$ for the mean spectrum of $Q = 17$ μK, $n = 1$ inputs is caused by the off-diagonal response to $\ell = 3$, while the off-diagonal response of $\ell = 4$ to $\ell = 2$ has been zeroed by the MDQ method. For a model power spectrum C_ℓ, the expected values

[7] The full matrix for ℓ', $\ell \leq 30$ can be found at http://www.astro.ucla.edu/~wright/pspct4yr_full_table_1.txt.

TABLE 1

$\frac{10^3}{2\ell' + 1} \sum_m T_{\ell^2} \{F_{\ell' m}\}$ FOR THE CUSTOM GALAXY CUT

	ℓ							
ℓ'	2	3	4	5	6	7	8	9
0	0	0	0	0	0	0	0	0
1	0	0	0	0	0	0	0	0
2	1087	0	0	0	0	0	0	0
3	0	1016	0	275	1	84	1	21
4	150	0	930	0	295	1	81	1
5	0	197	1	1067	0	182	1	63
6	35	0	251	0	1051	1	179	1
7	0	46	1	138	0	1103	1	167
8	6	0	55	0	143	1	1100	1
9	0	9	1	38	0	132	1	1105

NOTE.–$T_{\ell^2}\{F_{\ell' m}\}$ is the Hauser-Peebles power spectrum of the unit variance real spherical harmonic $F_{\ell' m}$ defined in Wright et al. 1994b.

of the Hauser-Peebles spectral estimators in the cut sky are $\langle T_\ell^2 \rangle = \sum (2\ell' + 1)V(\ell', \ell)G_{\ell'}^2 C_{\ell'}/4\pi$, where G_ℓ is the DMR beam response from Wright et al. (1994b) and V is taken from Table 1 (divided by 1000).

This method computes the power spectrum, a quadratic function of the map, which includes contributions from both the true sky signal and from instrument noise. We remove the contribution of the instrument noise by subtracting the power spectrum of a noise only map. This difference map can be constructed by subtracting the two maps made from the A and B sides of the DMR instruments: $D = (A - B)/2$. The sum

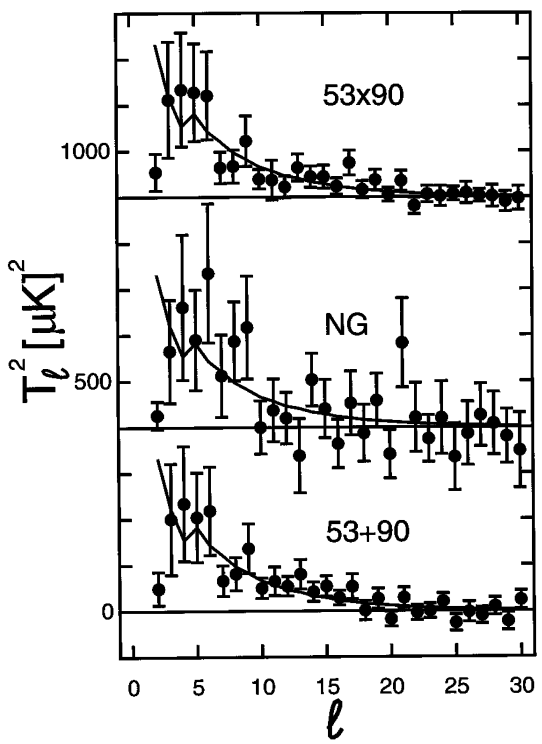

FIG. 1.—Cross-power spectra for the 53 + 90 $A \times B$, 53 × 90, and NG $A \times B$ maps. T_ℓ^2 measures the variance of the sky due to order ℓ harmonics for full sky coverage, but partial sky coverage changes the expected value as seen in the curves showing the average power spectrum of $Q = 17$ μK, $n = 1$ Monte Carlo models in the cut sky. Values are shifted upward by 400 for NG and 900 for 53 × 90, as shown by the horizontal lines marking zero power.

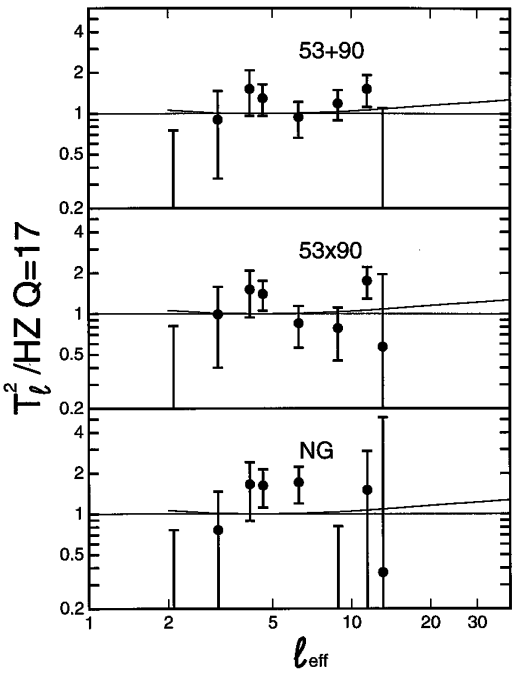

FIG. 2.—Binned cross-power spectra for the 53 + 90 $A \times B$, 53 × 90, and NG $A \times B$ maps, normalized to the mean power spectrum of $Q = 17$ μK, $n = 1$ simulations, plotted on a logarithmic scale. ℓ_{eff} is the effective wavenumber of the bin for $n = 1$. The thin curves show a CDM model with $n_{pri} = 0.96$ including the effect of gravitational waves derived from Crittenden et al. (1993).

map containing the real signal is $S = (A + B)/2$. When we compute the quadratic power spectrum, we use the value $S^2 - D^2 = A \times B$, so the power spectra reported here are the cross-power spectra between the A and B sides of the DMR instrument.

We have computed the power spectrum of the internal linear combination "free-free" no-galaxy (NG) map (Wright et al. 1994a), $T_{NG} = -0.4512T_{31} + 1.2737T_{53} + 0.3125T_{90}$, and the close to maximum signal-to-noise ratio maps based on $0.6T_{53}/0.931 + 0.4T_{90}/0.815$. The denominators in the latter expression convert the Rayleigh-Jeans differential temperatures T_{53} and T_{90} into thermodynamic ΔT's, but this conversion is included in the coefficients for T_{NG}. This process can also be applied to compute the cross-power spectrum of the 53 GHz and 90 GHz maps by letting $S = (53 + 90)$ and $D = (53 - 90)$, after both maps have been converted into thermodynamic brightness temperature differences. Figure 1 shows the resulting power spectra for the three map combinations.

We have binned the power spectra in quasi-logarithmic bins in ℓ in order to minimize the increasing noise-to-signal ratio as ℓ gets large. Figure 2 and Table 2 show these binned power-spectral estimates.

3. MONTE CARLO SIMULATIONS

In order to calibrate and test these methods for biases, it is necessary to simulate both the *cosmic variance*, which gives a random map with random spherical harmonic amplitudes chosen from a Gaussian distribution with a variance determined from the chosen Q_{in} and n_{in}, and the *experimental variance*, which gives the 360 million noise values needed yr^{-1}.

TABLE 2

BINNED POWER SPECTRA OF FOUR-YEAR DMR MAPS

ℓ Range	ℓ_{eff}	NG $A \times B$	53 × 90	53 + 90 $A \times B$
2	2.1	0.08 ± 0.68	0.16 ± 0.65	0.15 ± 0.60
3	3.1	0.76 ± 0.70	0.99 ± 0.59	0.90 ± 0.57
4	4.1	1.65 ± 0.76	1.51 ± 0.57	1.52 ± 0.56
5–6.....	4.6	1.62 ± 0.51	1.40 ± 0.35	1.30 ± 0.34
7–9.....	6.3	1.71 ± 0.52	0.85 ± 0.29	0.94 ± 0.28
10–13	8.9	−0.02 ± 0.79	0.78 ± 0.33	1.19 ± 0.30
14–19	11.5	1.50 ± 1.42	1.75 ± 0.46	1.52 ± 0.40
20–30	13.2	0.37 ± 4.81	0.57 ± 1.39	0.02 ± 1.08

NOTE.—All values have been normalized to the mean for $Q = 17$ μK, $n = 1$ Monte Carlo runs.

The effect of noise on the map production process can be simulated using

$$T_n = \sigma_1 A^{-0.5} U, \quad (5)$$

where σ_1 is the noise in one observation, U is an uncorrelated vector of unit variance zero mean Gaussian random variables, and A is the matrix with diagonal elements A_{ii} equal to the number of times the ith pixel was observed, and off-diagonal elements $-A_{ij}$ equal to the number of times the ith pixel was referenced to the jth pixel. Even though A is singular, Wright et al. (1994a) give a rapidly convergent series technique for generating noise maps. Thus, each noise map depends on 6144 independent Gaussian unit variance random variables and the parameter σ_1.

The signal map that is added to the noise maps to give the "observed" maps is generated using independent Gaussian random amplitudes with variances given by Bond & Efstathiou (1987) for $\ell < 40$. The simulations done here included ℓ's up to 39, so the signal map depends on 1600 Gaussian independent unit variance random variables and the two parameters Q_{in} and n_{in}. Note that while we use N_{obs} in generating the Monte Carlo noise maps, both the Monte Carlo maps and the real maps are analyzed using exactly the same functions $G'_{\ell m}$ which are derived without considering the N_{obs} weights. In fact, the Monte Carlo maps and the real maps are analyzed using exactly the same computer program.

4. MAXIMUM LIKELIHOOD ESTIMATION

Using the Monte Carlos, we find the mean power spectrum $\overline{T_\ell^2}(Q_{in}, n_{in})$, and the covariance matrix $C(Q_{in}, n_{in})_{\ell\ell'} = \langle (T_\ell^2 - \overline{T_\ell^2})(T_{\ell'}^2 - \overline{T_{\ell'}^2}) \rangle$. For the actual power spectrum T_ℓ^2 from the real sky or a Monte Carlo simulation, we define the deviation vector $e_\ell = T_\ell^2 - \overline{T_\ell^2}(Q_{in}, n_{in})$ and the χ^2 statistic, $\chi^2 = e^T C^{-1} e$. All of the fits in this paper are based on the range $\ell = \ell_{min}$–ℓ_{max}, with $\ell_{min} = 3$ and $\ell_{max} = 30$. C is thus a 28 × 28 matrix. Ignoring the quadrupole is reasonable because the Galactic corrections are largest for $\ell = 2$, and the maximum order used is set by the DMR beam size of 7° and the increased computer time required to analyze more orders. Since the magnitude of the covariance matrix gets larger rapidly when Q_{in} increases, there is a bias toward large values of Q when minimizing χ^2. One can allow for this by minimizing $-2 \ln L$ instead of χ^2, where L is the Gaussian approximation to the likelihood:

$$-2 \ln L = \chi^2 + \ln (\det C) + \text{const}. \quad (6)$$

For any given power spectrum, we can adjust Q_{in} and n_{in} until $-2 \ln L$ is minimized. This gives us the maximum likeli-

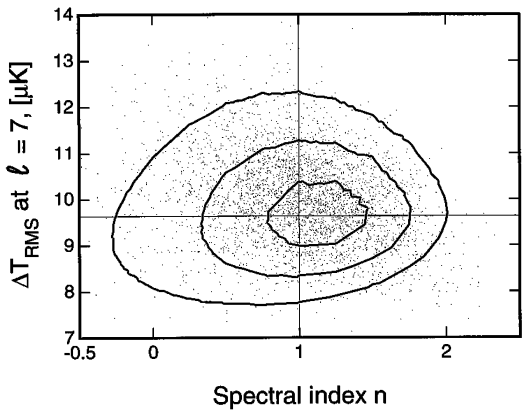

FIG. 3.—Each point is an input parameter set that is consistent with the real 4 yr 53 × 90 DMR data for a given realization of the random cosmic and radiometer variance processes. Amplitude is specified using the RMS ΔT due to $\ell = 7$ spherical harmonics because $\ell_{\rm eff}$ for this fit is 7.3. The likelihood contours are at $\Delta(-2 \ln L) = 1$, 4, and 9.

hood fit of a power-law power spectrum to the given power spectrum. We have called the values of Q and n that maximize the likelihood for the observed power spectrum $Q_{\rm ML}$ and $n_{\rm ML}$ since these are maximum likelihood values. The maximum likelihood technique gives an *asymptotically* unbiased determination of the amplitude Q and index n, but only as the observed solid angle goes to infinity. Since we are limited to about 8 sr of sky, asymptotically unbiased means *biased* in practice, both for the quadratic statistics considered here and for linear statistics used by Górski et al. (1994) and Bond (1995). Our use of a Gaussian approximation to the likelihood for our quadratic statistics can introduce additional errors. We use our Monte Carlo simulations to calibrate our statistical methods to avoid biased final answers.

Our kth Monte Carlo run depends on a set of random variables $\{Z_k\}$ (with 1600 + 12288 elements for a cross-analysis needing two noise maps) having a known distribution, and the three parameters $Q_{\rm in}$, $n_{\rm in}$, and σ_1. σ_1 can be determined with great precision using the time-ordered data. Hence one needs to run many Monte Carlo simulations with several different values for $Q_{\rm in}$ and $n_{\rm in}$ and compare the fitted values $Q_{{\rm ML},k}$ and $n_{{\rm ML},k}$ to the fitted values for the real data, $Q_{\rm ML,obs}$ and $n_{\rm ML,obs}$. For the kth realization $\{Z_k\}$, the fitted values $Q_{{\rm ML},k}$ and $n_{{\rm ML},k}$ are a continuous function of the input parameters $Q_{\rm in}$ and $n_{\rm in}$, and one can choose values $Q_{\rm in} = Q_{{\rm match},k}$ and $n_{\rm in} = n_{{\rm match},k}$ such that $Q_{{\rm ML},k} = Q_{\rm ML,obs}$ and $n_{{\rm ML},k} = n_{\rm ML,obs}$. By choosing many different realizations of $\{Z_k\}$, one creates many different $(Q_{\rm match}, n_{\rm match})$ pairs. Figure 3 shows this cloud of points for the 53 × 90 cross-power spectrum, along with contours of $-2 \ln L$. The spectral index we give is the median of the set of $n_{\rm match}$'s, and the 16th percentile to 84th percentile range in $n_{\rm match}$ defines the ± 1 σ range. The value $1.13^{+0.3}_{-0.4}$ given in the abstract is the weighted mean of these determinations, but we have not reduced the error because the cosmic variance is common to all three maps.

TABLE 3

POWER-LAW FITS TO FOUR-YEAR DMR MAP POWER SPECTRA

Maps	$n_{\rm app}$	$\langle Q^2_{\rm rms}\rangle^{0.5}$ at $n_{\rm app} = 1$ (μK)
53 + 90 $A \times B$	$1.17^{+0.34}_{-0.41}$	$17.9^{+1.6}_{-1.6}$
53 × 90	$1.02^{+0.44}_{-0.47}$	$17.3^{+1.6}_{-2.1}$
NG $A \times B$	$1.22^{+0.60}_{-0.71}$	$19.6^{+2.9}_{-2.6}$

The value of $\langle Q^2_{\rm rms}\rangle^{0.5}$ can be found by doing a one-parameter maximum likelihood fit for $Q_{\rm ML}$ with n fixed at 1. After using the Monte Carlo runs to debias the maximum likelihood results, we get the values shown in Table 3. We can also find the best-fit values of Q for other values of n. The best-fit Q values for n forced to be 1.25 are smaller than those for n forced to be 1 by an amount that allows us to estimate the effective wavenumber of our amplitude determination. We find that $\ell_{\rm eff} = 7.9$ for the 53 + 90 $A \times B$ case and 7.3 for the 53 × 90 case. In Figure 3 we have chosen to plot the amplitude at $\ell = 7$ which is closest to the effective wavenumber in order to minimize the correlation between the amplitude and the spectral index.

5. DISCUSSION

The angular power spectrum of the 4 yr *COBE* DMR maps has been calculated, and it is very consistent with a Harrison-Zeldovich primordial spectrum $n_{\rm pri} = 1$, especially after the small correction for the "toe" of the Doppler peak which gives an expected apparent index of $n_{\rm app} \approx 1.1$ for $\Omega = 1$ CDM models. Models with a cosmological constant (ΛCDM) predict a smaller $n_{\rm app} \approx 0.75$ (Kofman & Starobinsky 1985) that is still consistent with the *COBE* DMR observations. The amplitude derived from this analysis is in between the $\langle Q^2_{\rm rms}\rangle^{0.5} = 17$ μK derived from the first year maps and the $\langle Q^2_{\rm rms}\rangle^{0.5} = 19$ μK derived from the 2 yr maps (Wright et al. 1994a). The amplitude from the no-galaxy map is consistent with, but now slightly higher than, the amplitude derived from the 53 and 90 GHz maps, indicating that Galactic contamination is not a major problem with the new custom Galactic cut.

We are grateful for the efforts of the *COBE* team and the support of the Office of Space Sciences at NASA. Charley Lineweaver provided helpful comments on an early draft of this paper.

REFERENCES

Bardeen, J. M., Steinhardt, P. J., & Turner, M. S. 1983, Phys. Rev. D, 28, 679
Bennett, C. L., et al. 1992, ApJ, 396, L7
———. 1996, ApJL, 464, L1
Bond, J. R. 1995, Phys. Rev. Lett., 74, 4369
Bond, J. R., & Efstathiou, G. 1987, MNRAS, 226, 655
Crittenden, R., Bond, J. R., Davis, R. L., Efstathiou, G., & Steinhardt, P. J. 1993, Phys. Rev. Lett., 71, 324
Górski, K. M., Hinshaw, G., Banday, A. J., Bennett, C. L., Wright, E. L., Kogut, A., Smoot, G. F., & Lubin, P. 1994, ApJ, 430, L89
Guth, A. 1981, Phys. Rev. D, 23, 347
Harrison, E. R. 1970, Phys. Rev. D, 1, 2726
Hauser, M. G., & Peebles, P. J. E. 1973, ApJ, 185, 757
Kofman, L. A., & Starobinsky, A. A. 1985, Soviet Astron. Lett., 11, 271
Peebles, P. J. E. 1973, ApJ, 185, 413
Peebles, P. J. E., & Yu, J. T. 1970, ApJ, 162, 815
Starobinsky, A. A. 1980, Phys. Lett. B, 91B, 99
Wright, E. L., Smoot, G. F., Bennett, C. L., & Lubin, P. M. 1994a, ApJ, 436, 443
Wright, E. L., Smoot, G. F., Kogut, A., Hinshaw, G., Tenorio, L., Lineweaver, C., Bennett, C. L., & Lubin, P. M. 1994b, ApJ, 420, 1
Zeldovich, Y. B. 1972, MNRAS, 160, 1P